THE JOURNAL OF BIOLOGICAL CHEMISTRY VOL. 291, NO. 42, pp. 21903–21912, October 14, 2016

Alternative Processing of the Amyloid Precursor Protein Family by Rhomboid Protease RHBDL4*

Received for publication, August 15, 2016, and in revised form, August 24, 2016 Published, JBC Papers in Press, August 25, 2016, DOI 10.1074/jbc.M116.753582

Sandra Paschkowsky[‡], Mehdi Hamzé[‡], Felix Oestereich[‡§], and Lisa Marie Munter[‡1]

From the [‡]Department of Pharmacology and Therapeutics and [§]Integrated Program in Neuroscience, McGill University, Montreal, Quebec H3G 0B1, Canada

The amyloid precursor protein (APP) is an ubiquitously expressed cell surface protein and a key molecule in the etiology of Alzheimer disease. Amyloidogenic processing of APP through secretases leads to the generation of toxic amyloid β (Aβ) peptides, which are regarded as the molecular cause of the disease. We report here an alternative processing pathway of APP through the mammalian intramembrane rhomboid protease RHBDL4. RHBDL4 efficiently cleaves APP inside the cell, thus bypassing APP from amyloidogenic processing, leading to reduced Aβ levels. RHBDL4 cleaves APP multiple times in the ectodomain, resulting in several N- and C-terminal fragments that are not further degraded by classical APP secretases. Knockdown of endogenous RHBDL4 results in decreased levels of C-terminal fragments derived from endogenous APP. Similarly, we found the APP family members APLP1 and APLP2 to be substrates of RHBDL4. We conclude that RHBDL4-mediated APP processing provides insight into APP and rhomboid physiology and qualifies for further investigations to elaborate its impact on Alzheimer disease pathology.

The amyloid precursor protein (APP)[2] is abundantly expressed throughout the human body and shows high levels in the brain, lung, and liver (1). APP is a type I transmembrane protein that undergoes complex glycosylation and trafficking to the cell surface. Several physiological functions for APP have been reported, including involvement in cell adhesion and migration, proliferation, and cholesterol and copper homeostasis (2–4). In the brain, APP is required for neuronal development and synaptic maintenance (5–7), although the detailed mechanisms underlying these effects remain unclear. In addition to APP itself, the APP family also comprises the homologous APP-like proteins 1 and 2 (APLP1 and APLP2), which show partial functional redundancy (8). All APP family members undergo ectodomain shedding through the action of matrix metalloproteases (α-secretase) or β-site APP cleaving enzyme 1 (BACE1) (9, 10). Then, in a second step, the remaining membrane-bound stubs are processed by γ-secretase (11). Sequential cleavage of APP by BACE1 and γ-secretase results in the generation of harmful amyloid β (Aβ) peptides, which are proposed as the molecular cause of Alzheimer disease (12). γ-Secretase is an intramembrane protease and cleaves the APP transmembrane sequence at multiple sites, generating Aβ peptides with predominantly 38, 40, and 42 amino acids, which are secreted (13).

Besides γ-secretase, other classes of intramembrane proteases are known, including the superfamily of rhomboid proteases (14). Rhomboid proteases are evolutionarily conserved and found in all kingdoms of life, including archaea, prokaryotes, plants, and animals (15, 16). Such conservation suggests that they successfully withstood evolutionary pressure and carry out essential biological functions. Defining rhomboid protease functions strongly depends on the identification of their substrates, which has been difficult so far. In mice and humans, proteolytically active and inactive rhomboid protein family members have been linked to EGF and TNFα signaling (17–23). Furthermore, the mitochondrial rhomboid protease presenilins-associated rhomboid-like protein (PARL) has been implicated in mitophagy (24) and is linked to Parkinson disease (25, 26). Active rhomboid proteases directly recognize their substrates and do not require an initiating ectodomain shedding event, unlike γ-secretase (27). Substrate cleavage occurs within the transmembrane sequence, but cleavage events in extramembrane regions have also been described (28–31). In addition to PARL, there are four other active rhomboid proteases known in humans, *i.e.* RHBDL1, 2, 3, and 4 (32).

Here we show that the APP family members are efficient substrates for the rhomboid protease RHBDL4. RHBDL4-mediated cleavage of APP leads to the generation of multiple APP N- and C-terminal fragments intracellularly, resulting in a significant decrease of secreted Aβ peptide levels. We propose that processing of APP by RHBDL4 is an alternative APP processing pathway, maybe functioning to regulate levels of APP presented at the cell surface, which may further our understanding of APP biology.

Results

RHBDL4 Cleaves APP—To investigate whether rhomboid proteases cleave APP, we co-expressed RHBDL1, 2, 3, or 4 with full-length APP695 in HEK 293T cells. Full-length APP levels,

* This work was supported by Natural Sciences and Engineering Research Council of Canada (NSERC) Discovery Grant RGPIN-2015-04645, the Canada Foundation of Innovation Leaders Opportunity Fund Grant 32565, Alzheimer Society of Canada Young Investigator Award PT-58872, Fonds d'innovation Pfizer-Fonds de recherche Santé Québec (FRQS) sur la maladie d'Alzheimer et les maladies apparentées 31288, McGill University Startup funding, and McGill Faculty of Medicine Incentive funding. The authors declare that they have no conflicts of interest with the contents of this article.

[1] To whom correspondence should be addressed: E-mail: lisa.munter@mcgill.ca.

[2] The abbreviations used are: APP, amyloid precursor protein; Aβ, amyloid β; PARL, presenilins-associated rhomboid-like protein; sAPP, soluble amyloid precursor protein; CTF, C-terminal fragment; ER, endoplasmic reticulum; ERAD, endoplasmic reticulum-associated degradation; Tricine, *N*-[2-hydroxy-1,1-bis(hydroxymethyl)ethyl]glycine; fl, full-length; ALLN, Ac-Leu-Leu-Nle-al.

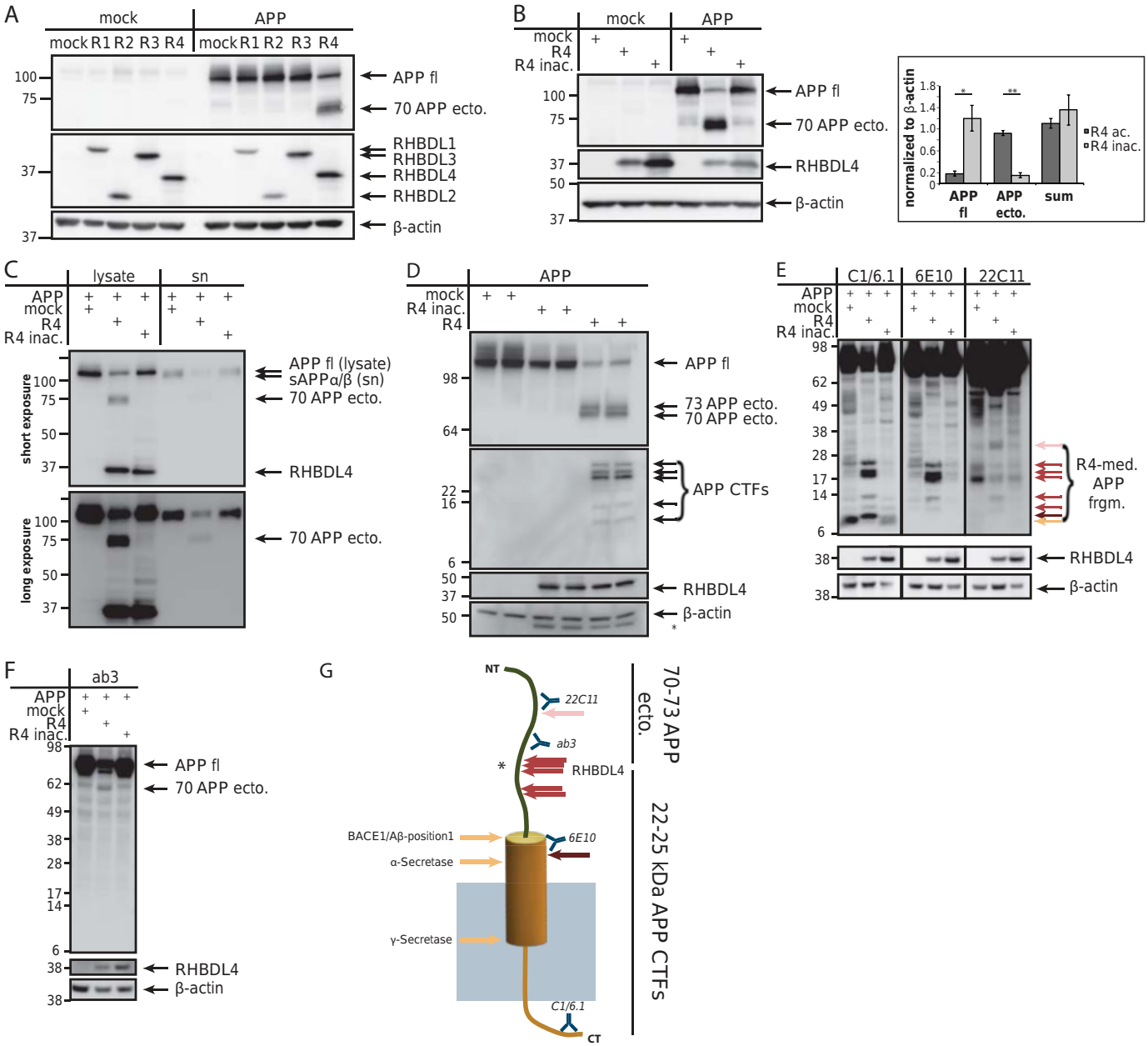

FIGURE 1. **RHBDL4-mediated APP processing.** *A*, co-expression of APP and rhomboid proteases in HEK 293T cells. A stable 70-kDa APP ectodomain (*ecto*) fragment was observed in cell lysates only with co-expression of RHBDL4. Shown is a representative Western blot of three independent experiments. *B*, inactive RHBDL4 S144A (*R4 inac*) showed no APP cleavage. APP full-length (fl) and the 70-kDa fragment were quantified and normalized to β-actin (see graph). The sum of APP fl and fragment revealed no significant difference between active (*ac*) and inactive RHBDL4. Mean ± S.E., $n = 4$, two-tailed paired *t* test. *, $p < 0.05$; **, $p < 0.01$. *C*, secretion of ectodomain fragment. 36 h after transient transfection, the cell culture supernatant was conditioned for 12 h containing 5% FCS. APP carries an N-terminal myc tag and was detected with anti-myc antibody from the lysate and supernatant. Secreted sAPPα/β migrates at about 110 kDa and is detected in the supernatant (*sn*). The signal at 36 kDa represents RHBDL4 (myc-tagged). Shown is a representative Western blot of three independent experiments. *D*, generation of large APP-CTFs. *Top panel*, higher resolving gel showing that the RHBDL4-mediated 70-kDa APP ectodomain fragment in lysate migrates as a double band at 70 and 73 kDa. Multiple APP CTFs in the range of 10–25 kDa were detected with antibody 6E10. The *asterisk* indicates RHBDL4 staining from the panel above. Shown is a representative Western blot of four independent experiments. *E*, for detailed analysis of APP fragments, samples from the experiments in *D* were reblotted in *E* and stained with different antibodies. The same samples were loaded three times on the same gel. Blots were cut before staining with C1/6.1, 6E10, or 22C11 as indicated. The *light red arrow* indicates the 22C11-reactive APP fragment, *medium red arrows* indicate 6E10- and C1/6.1-reactive fragments, and the *dark red arrow* indicates only C1/6.1-reactive fragment. The *yellow arrow* indicates α-CTF that is present in the mock control. Shown is a representative Western blot of three independent experiments. *F*, the antibody ab3 does not stain CTFs but the 70-kDa APP ectodomain fragment and APP fl. Shown is a representative Western blot of at least two independent experiments. *G*, schematic of APP cleavage sites. According to the size of RHBDL4-mediated APP fragments (indicated on the *right*), RHBDL4 cleaves multiple times in the APP ectodomain N- and C-terminal of the BACE1 cleavage site. The *asterisk* indicates the presumed preferential cleavage sites. The arrow color code is according to *E*. Also indicated are the binding sites of APP antibodies 22C11 (APP ectodomain, residues 66–81), ab3 (465–514 of APP695), 6E10 (Aβ region, residues 3–8), and C1/6.1 (676–695 of APP695). The *cylinder* indicates the Aβ peptide region with new amino acid numbering starting at the BACE1 cleavage site with 1. *A–F*, detection of APP was performed with 22C11 unless indicated otherwise and of RHBDL4 with anti-myc antibody, and β-actin was used as a loading control.

detected at about 100 kDa, were not affected by RHBDL1, 2, or 3 (Fig. 1*A*). However, co-expression with RHBDL4 resulted in a robust decrease in the levels of full-length APP. In addition, a 70-kDa APP N-terminal fragment was detected in the cell lysate (Fig. 1*A*). This fragment was smaller than the soluble APP ectodomain fragments generated by α-secretase or BACE1 cleavage, and likely corresponded to a distinct ectodomain fragment. To determine whether this cleavage was specific for proteolytic activity of RHBDL4, we generated an inactive RHBDL4 mutant by exchanging the catalytically active serine in position 144 for an alanine residue (S144A) (33). When expressing the inactive RHBDL4 S144A mutant with APP, the expression of full-length APP was restored, and, in accordance, no 70-kDa fragment was generated (Fig. 1*B*). Compared with the inactive mutant, active RHBDL4 significantly decreased full-length APP levels by 82.8% ± 6.1% (Fig. 1*B*). Comparing the signal intensities of the sum of full-length and the 70-kDa APP fragment of the active *versus* inactive RHBDL4 variant revealed a trend toward a slightly smaller sum for active RHBDL4, which was not significant (Fig. 1*B* quantification). This indicates that the decrease of full-length APP is almost compensated by the increase of the 70-kDa fragment (Fig. 1*B*). We therefore hypothesized that a proportion of this fragment may be secreted.

To investigate the cellular fate of the 70-kDa APP ectodomain fragment, we analyzed the cell culture supernatant for its presence. Indeed, we detected this fragment only from cells expressing active RHBDL4 but not the inactive form or mock control (Fig. 1*C*), indicating that it is secreted. In addition, the antibody used in this Western blot recognizes secreted soluble APP ectodomain fragments generated through α-secretase and BACE1 (sAPPα/β) in the supernatant. With active RHBDL4, sAPPα/β levels are much lower in the supernatant than with inactive RHBDL4, indicating that classical APP processing is circumvented. Importantly, using a gel system that separates high molecular weight proteins, we noted that the RHBDL4-mediated 70-kDa fragment appeared as a double band (apparent molecular weight, 70 and 73 kDa; Fig. 1*D*, *top panel*), which may represent different cleavage products. The presence of these 70- to 73-kDa APP fragments raised the question as to whether RHBDL4 also generates corresponding APP C-terminal fragments (CTFs). Analysis of cell lysates with gels separating low molecular weight proteins revealed that RHBDL4 generates at least five APP C-terminal fragments between 10- to 25-kDa sizes, with the most prominent band at around 21 kDa (depending on the gel system and marker used, Fig. 1*D*). None of these cleavage fragments were detected with inactive RHBDL4 (Fig. 1*D*). The use of multiple APP antibodies with different epitope specificities revealed at least three different regions where RHBDL4 cleaves APP (Fig. 1, *E–G*). We detected a 30-kDa fragment that was 22C11-reactive, an antibody that binds at position 66–81 in the APP ectodomain, indicating that RHBDL4 cleaves APP around amino acid 270. Furthermore, the use of 6E10, specific for the N-terminal Aβ region residues 3–8, revealed five fragments larger than β-CTF, indicating five cleavage sites N-terminal to the BACE1 site. Differential comparison of CTFs stained with C1/6.1, an antibody specific for the last 20 C-terminal amino acids of APP, *versus* 6E10 enabled us to localize at least one cleavage within the Aβ region, N-terminal of the α-secretase cleavage site but C-terminal of the 6E10 epitope (not 6E10-reactive, CTF larger than α-CTF). Of note, abundant α-secretase-derived α-CTFs and the more rare β-CTFs are detected with C1/6.1 (Fig. 1*E*, *first lane*). β-CTFs can be distinguished from α-CTFs using the antibody 6E10; however, under our experimental conditions, β-CTFs are not detected, probably because of a relatively low amount of protein loaded on the gels to be able to resolve the RHBDL4-derived CTFs that give strong Western signals (Fig. 1, *D* and *E*, *center panels*). In addition, the antibody ab3 recognizing an ectodomain epitope (residues 465–514) did not detect any RHBDL4-mediated CTFs but the 70-kDa ectodomain fragment, implying that the APP C-terminal fragments do not contain the ab3 epitope (Fig. 1*F*). All potential RHBDL4-mediated cleavages in APP are summarized in Fig. 1*G*.

Cleavage of Endogenous APP—To gain more insight into the physiology of RHBDL4-mediated APP cleavage, we took advantage of the endogenous expression of APP in the human neuroblastoma cell line SH-SY5Y. Overexpression of active RHBDL4 resulted in the generation of an endogenous APP ectodomain fragment (Fig. 2*A*) similar to the ones observed in the co-expression experiments (Fig. 1). Likewise, HEK 293T cells endogenously express the larger APP isoform APP751 detectable at higher molecular weights than APP695, *i.e.* at 120 kDa, because of an additional domain in this isoform. Titrating increasing amounts of active RHBDL4 resulted in increasing levels of endogenous APP N- and C-terminal fragments (Fig. 2*B*). Quantification of endogenous 75-kDa fragments (slightly higher than the fragment from APP695, as expected) reveals a correlation between fragment levels and amounts of transfected RHBDL4 cDNA (Fig. 2*B*). Thus, endogenous APP is cleaved in a concentration-dependent manner by RHBDL4.

Next, we aimed to investigate the fate of these endogenous APP CTFs. In a recent publication by Wang *et al.* (34), the accumulation of novel, larger APP CTFs upon ALLN treatment, a lysosomal inhibitor, was described (34). We were also able to accumulate such CTFs in wild-type HEK 293T cells (Fig. 2*C*). Similarly, when expressing RHBDL4, the signals for endogenous APP CTFs increased and were further accumulated by ALLN treatment (Fig. 2*C*). Comparison of the RHBDL4-mediated CTFs and CTFs described by Wang *et al.* (34) shows that the CTF pattern is partially overlapping, implying that at least some of the CTFs that accumulate with ALLN in wild-type cells may derive from endogenous RHBDL4 processing. To further investigate this idea, we down-regulated endogenous RHBDL4 levels using shRNAs (Fig. 2*D*). We observed that, with decreasing RHBDL4 levels, the signals for the endogenous APP-CTF at 10 kDa were reduced as well. Additional treatment with ALLN demonstrated again the accumulation of endogenous APP CTFs up to 15 kDa under control conditions but not under RHBDL4 knockdown conditions (Fig. 2*D*). Quantified RHBDL4 knockdown efficiency correlated with a decrease of the 10- to 15-kDa CTF levels (Fig. 2*D*).

APP-RHBDL4 Interaction—To further study RHBDL4 and APP as an enzyme-substrate pair, we first analyzed their interaction using co-immunoprecipitation. Using an APP-specific antibody (6E10), we pulled down full-length APP and co-immunoprecipitated inactive RHBDL4 (Fig. 2*E*). Less active

RHBDL4 was co-immunoprecipitated, as expected, because the enzyme likely processes APP upon binding (Fig. 2*E*, *bottom panel*).

In Western blots, APP migrates as two predominant bands representing the immature, core glycosylated APP residing in the endoplasmic reticulum (ER) (Fig. 2*F*, *bottom band*) and the mature protein at the cell surface (Fig. 2*F*, *top band*). Furthermore, Fleig *et al.* (33) described that RHBDL4 localizes in the ER. Therefore, we wanted to determine the subcellular localization of the APP-RHBDL4 interaction by titrating increasing amounts of inactive RHBDL4 with a constant amount of APP cDNA. The results showed an increase of immature APP levels the more inactive RHBDL4 was expressed (Fig. 2*F*). This indicates that APP is retained in the ER by inactive RHBDL4, which could be explained if inactive RHBDL4 is still capable of binding APP but not able to proteolytically process it. Considering that the 70-kDa APP N-terminal fragments were observed in cell lysates, we rationalized that RHBDL4 interacts with and cleaves APP in the ER.

Analysis of Novel RHBDL4-mediated APP Fragments—Because APP is processed by α-secretase, BACE1, and γ-secretases, we investigated whether the RHBDL4-mediated cleavage

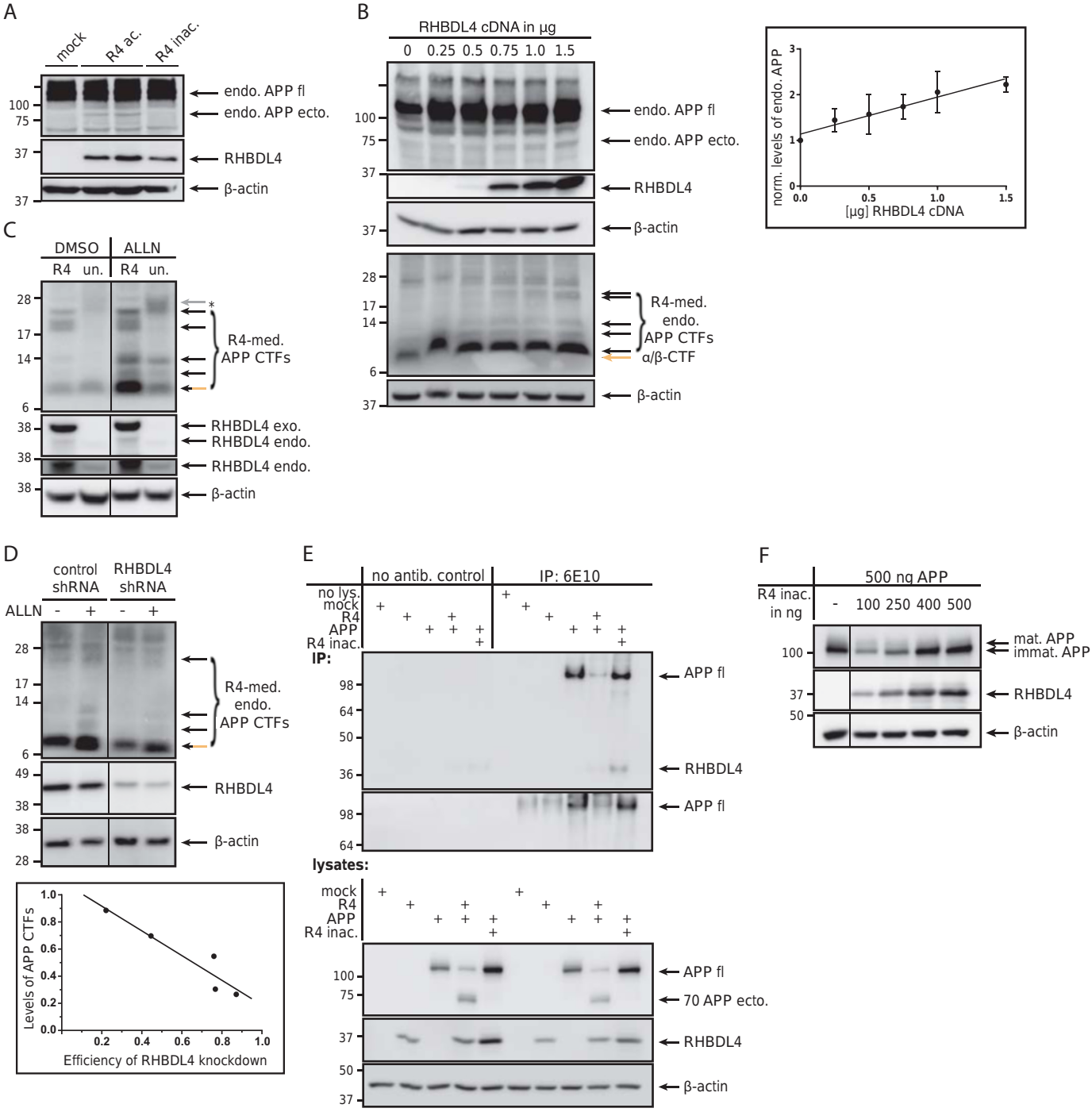

fragments were indeed generated independently of these enzymes or whether they were further degraded by them. Hence, we treated cells with various protease inhibitors. A matrix metalloprotease inhibitor (BB94) also inhibiting α-secretase led to a decrease in sAPPα, as expected, when only APP was expressed (Fig. 3*A*). However, upon co-expression with RHBDL4, no effects were observed on the APP ectodomain fragments or CTFs. Likewise, a BACE1 inhibitor successfully prevented the generation of sAPPβ in APP-transfected cells but had no effect on the generation of RHBDL4-mediated APP fragments (Fig. 3*B*). BACE1 inhibition also caused an accumulation of CTFs under control conditions, implying that α-secretase probably compensates for BACE1, an effect that depends on the cell type and protein overexpression of the specific experiment (35). Inhibition of γ-secretase resulted in the expected accumulation of α- or β-CTFs in controls but did not affect RHBDL4-derived N- or C-terminal APP fragments (Fig. 3*C*). Note that α- or β-CTFs do not accumulate when active RHBDL4 is co-expressed (Fig. 3*C*). This indicates that RHBDL4 prevents APP from processing through α- or β-secretase, which is in accordance with low levels of sAPP in the presence of active RHBDL4 (Figs. 1*C* and 3, *A* and *B*). In addition, we used broadband inhibitors for cysteine proteases (E64D), metalloproteases (phenanthroline), and aspartyl proteases (pepstatin A) (Fig. 3, *D–F*). None of these treatments affected the pattern of RHBDL4-mediated APP fragments. Thus, the inhibitor results indicate that these newly discovered APP fragments derive from RHBDL4-mediated APP processing and are neither generated nor degraded by classical secretases and likely not by other proteases.

RHBDL4-mediated Processing of APP Family Members—Based on the homology of the APP family members, we analyzed whether RHBDL4 also cleaves APLP1 and APLP2. Full-length APLP1 and APLP2 protein levels were reduced by 58% ± 9% and 71% ± 9%, respectively, when co-expressed with RHBDL4 in comparison with the inactive mutant (Fig. 4, *A*, *B*, and *E*). Notably, APLP1 and APLP2 generated two new ectodomain fragments at around 60 and 70 kDa and 80 and 100 kDa, respectively, similarly to APP (Fig. 4, *A* and *B*). To confirm the substrate specificity of RHBDL4, we also tested whether BACE1, another type I transmembrane protein involved in Alzheimer disease, and the transferrin receptor 1 (TfR) are cleaved by RHBDL4. Importantly, there were no signs of cleavage fragments for BACE1 or TfR (Fig. 4, *C* and *D*).

RHBDL4 Activity Reduces Aβ Peptide Levels—Finally, because Aβ peptides are a major hallmark of Alzheimer disease generated through amyloidogenic processing of APP, we investigated the impact of RHBDL4 on Aβ generation. We quantified Aβ38, Aβ40, and Aβ42 levels in conditioned cell culture supernatant of transfected cells using a multiplex ELISA. When comparing active RHBDL4 to the inactive mutant, we found Aβ38 levels to be decreased by 83% (Fig. 5*A*), Aβ40 by 69%, and Aβ42 levels by 57% (Fig. 5, *B* and *C*). Thus, RHBDL4 activity strongly reduces Aβ peptide levels. Taken together, because RHBDL4 processes APP likely in the ER and the RHBDL4-derived CTFs are not affected by γ-secretase, we conclude that RHBDL4-mediated APP cleavage is an alternative APP processing pathway bypassing the classical amyloidogenic pathway (Fig. 5*D*).

Discussion

Rhomboid proteases are a fascinating family of proteins with emerging roles in the immune system, cell proliferation, and cellular stress responses (18, 24, 33, 36, 37). To unravel rhomboid function, the identification of their substrates is critical. Here we show that APP family members are very good substrates of RHBDL4. Interestingly, RHBDL4 as an intramembrane protease cleaves APP multiple times within its ectodomain.

RHBDL4 has been linked with ER-associated degradation (ERAD) pathways and guides ubiquitinated substrates to the proteasome (33). Also, ERAD has been shown to be dysregulated in Alzheimer disease (38, 39). Therefore, we thought that RHBDL4 and APP may be linked via the ERAD machinery, and, indeed, we found APP efficiently cleaved by RHBDL4. However, we found no evidence that ubiquitination is required for RHBDL4-mediated APP cleavage events nor that larger APP CTFs are degraded by the proteasome.

FIGURE 2. **Cleavage of endogenous APP and RHBDL4-APP interaction.** *A*, SH-SY5Y cells were transfected with mock, active (*ac*), or inactive (*inac*) RHBDL4. Endogenous full-length APP and APP ectodomain (*ecto*) fragments were detected with the antibody LN27. Of note, the endogenous (*endo*) APP ectodomain fragment migrates slightly above the 75-kDa marker under these experimental conditions. Shown is a representative Western blot of three independent experiments. *B*, titration of increasing amounts of RHBDL4 cDNA as indicated in HEK 293T cells. Shown is a representative Western blot of the detection of endogenous APP and 75-kDa fragments ($n = 4$) as well as endogenous CTFs with C1/6.1 ($n = 3$). Note that the CTF signal in the control with 0 μg of RHBDL4 likely represents endogenous α- and β-CTFs (*yellow arrow*), whereas, in the following lanes with RHBDL4 transfection, the major CTF signal likely derives from RHBDL4-mediated (*R4-med*) APP processing (*lowest black arrow*). Levels of APP ectodomain fragments were quantified and normalized to actin with 0 μg set as 1 and are shown as a function of RHBDL4 cDNA levels. Shown is the mean ± S.E. *C*, detection of endogenous APP CTFs upon ALLN treatment. 36 h after transfection with RHBDL4 (untransfected as control), HEK 293T cells were treated with 50 μM ALLN (DMSO as vehicle control) for 12 h. 100 μg of total protein was separated by SDS-PAGE, and Western blots were stained with C1/6.1 for endogenous APP CTFs, rabbit-anti-RHBDL4 detecting exogenous (*exo*, short exposure, *second panel*) and endogenous RHBDL4 (*endo*, long exposure, *third panel*). Endogenous APP CTF signals are labeled with *black arrows* for RHBDL4-derived CTF, a *gray arrow* for a CTF signal that is probably not RHBDL4-mediated, and a *black/yellow mixed arrow* indicating potential co-migration of α-/β-CTFs. Shown is a representative Western blot of three independent experiments. *D*, down-regulation of endogenous RHBDL4 levels using shRNA. Cells expressing shRNAs were separated from non-transfected cells using FACS. Detection of endogenous APP CTFs was performed with C1/6.1 antibody. To enhance the endogenous APP CTF signal, HEK 293T cells were treated with 50 μM ALLN for 12 h (+). Signals for 10- to 15-kDa CTFs and RHBDL4 were quantified and normalized to β-actin. The graph shows levels of CTFs in relation to the knockdown efficiency of RHBDL4 (calculated by 1− (RHBDL4 shRNA/RHBDL4 control)). Each point represents one experiment ($n = 5$). Linear regression analysis: $Y = -0.9111 \times X + 1.099$, p (slope non-zero) = 0.0163. Note that the smallest RHBDL4-derived CTF signal decreases with RHBDL4 knockdown, but it may contain co-migrating α-/β-CTFs (*black/yellow-mixed arrow*). *E*, immunoprecipitation of full-length APP with 6E10 antibody. Negative controls were either no antibody (*antib*) or no lysate (*lys*). Particularly inactive RHBDL4 was co-immunoprecipitated with APP. The top immunoprecipitation blot was detected with anti-myc antibody for RHBDL4 and APP (N-terminal myc tag), and the bottom immunoprecipitation panel was detected with 6E10 also recognizing endogenous APP. Lysate blots below serve as expression controls. Shown is a representative Western blot of three independent experiments. *F*, titration of increasing amounts of inactive RHBDL4 (as indicated) and 500 ng of APP cDNA filled up to 2 μg of total DNA with empty vector. *mat*, mature; *immat*, immature. Shown is a representative Western blot of three independent experiments. *A–F*, if not stated differently, APP was detected with 22C11 and RHBDL4 with anti-myc antibody, and β-actin staining served as a loading control.

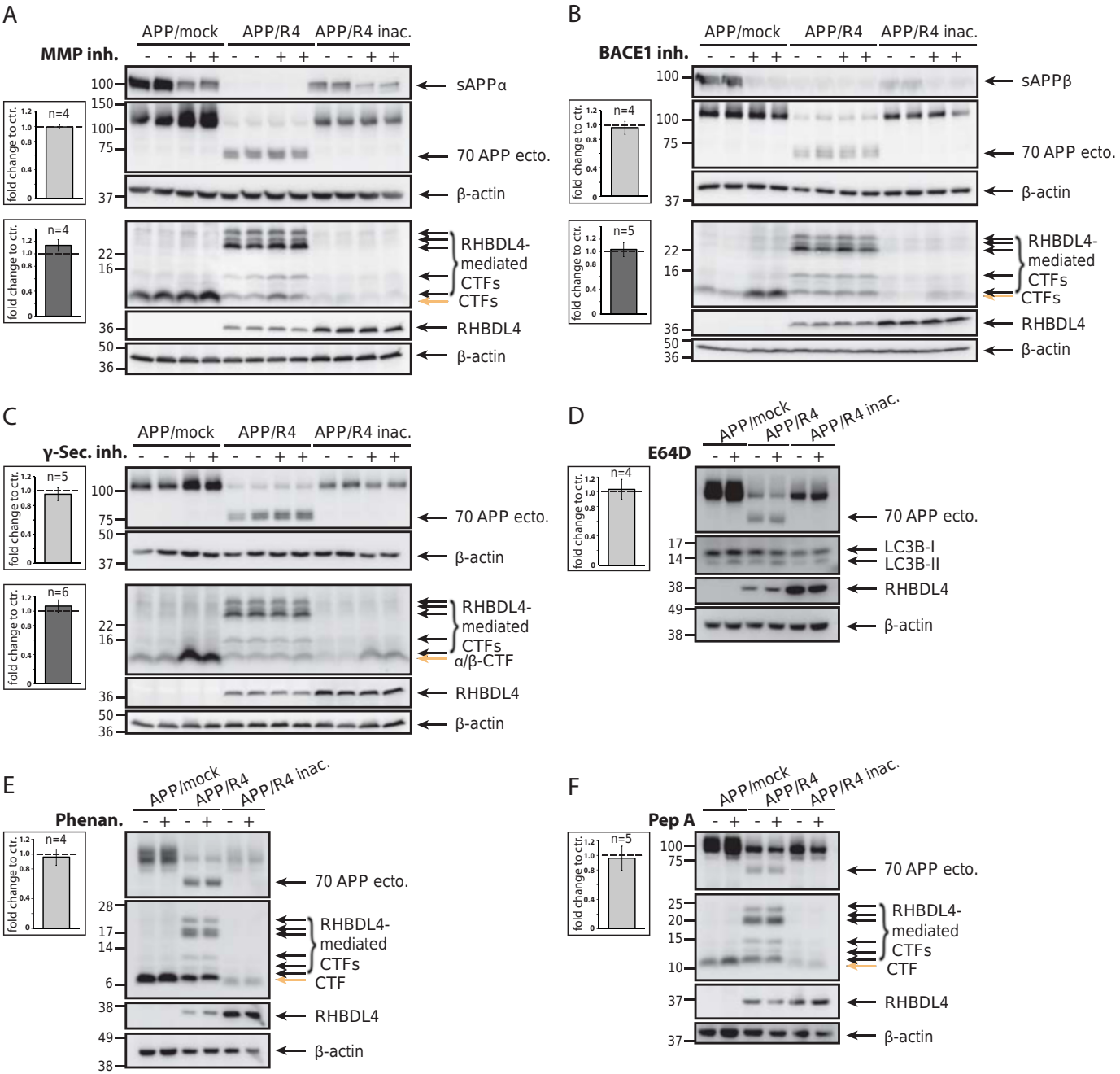

FIGURE 3. **RHBDL4-mediated APP fragments are neither generated nor degraded by α-secretase, BACE1, or γ-secretase.** *A–C*, *E*, and *F*, 36 h after transfection, cells were treated with matrix metalloprotease inhibitor (*A*, *MMP inh*, 10 μM BB94), BACE1 inhibitor (*B*, *BACE1 inh*, 1 μM inhibitor IV), γ-secretase inhibitor (*C*, *γ-Sec. Inh.*, 1 μM L685,485), metalloprotease inhibitor (*E*, 100 μM phenanthroline (*Phenan*)) and aspartyl protease inhibitor (*F*, 50 μM pepstatin A (*Pep A*)) for 12 h. *inac*, inactive; *ecto*, ectodomain. *D*, cells were treated with a cysteine protease inhibitor (10 μM E64D) for 24 h. DMSO was used as a vehicle control. APP was stained with 22C11, APP-CTFs with C1/6.1 (of note, this antibody does not differentiate between α- or β-CTF), sAPPα with 6E10, RHBDL4 with anti-myc antibody, and sAPPβ with a specific sAPPβ antibody. LC3B antibody staining as a positive control for E64D treatment showed an increase of the LC3B-II isoform (*bottom signal*). β-Actin was used as a loading control. Note that CTFs generated through classical APP processing by α- or β-secretase (*yellow arrow*, *CTFs*) migrate slightly lower than the smallest CTFs generated by RHBDL4 (*RHBDL4-mediated CTFs*). *A–F*, the N-terminal APP fragments were quantified as well as (for *A–C*) the 22- to 25-kDa APP CTFs (stained with either 6E10 or C1/6.1) and normalized to β-actin. *Error bars* depict the mean -fold change of inhibitor treatment ± S.E. compared with DMSO control (*ctr*) set as 1. The number of replicates is as indicated. All results were non-significant (two-tailed paired *t* test).

Previously, various APP N- and C-terminal fragments other than those generated by the three classical secretases have been found in different experimental contexts. APP N-terminal fragments between 17 and 28 kDa (22C11-reactive) have been described in the mouse brain by Vella and Cappai (40). Importantly, Wang *et al.* (34) have recently shown the existence of novel endogenous APP CTFs of 15- to 25-kDa size that were enriched after treatment with lysosomal inhibitors. We show here that RHBDL4 down-regulation results in a concomitant decrease of such APP CTFs, implying that at least some of the previously described APP fragments are generated through endogenous RHBDL4 activity.

Based on the fragment sizes, antibody-binding sites, and inhibitor studies, we showed that RHBDL4 cleaves APP at sev-

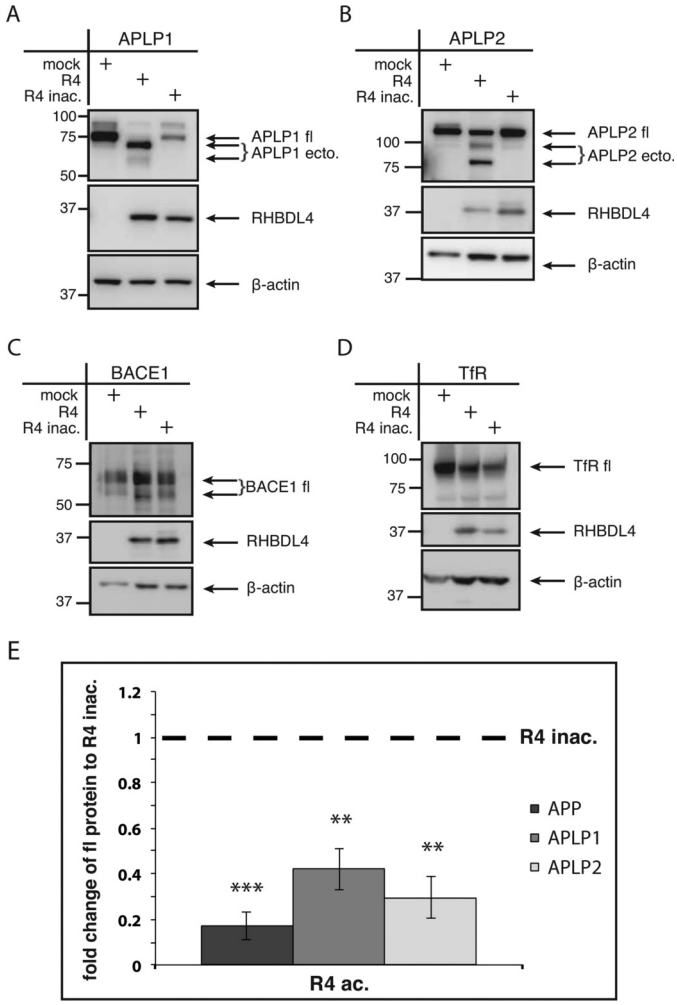

FIGURE 4. **RHBDL4 efficiently cleaves APP family members.** *A–D*, co-expression of APLP1 (*A*), APLP2 (*B*), BACE1 (*C*), or transferrin receptor 1 (*TfR*, *D*), with active (*ac*) or inactive (*inac*) RHBDL4. Blots were stained using specific antibodies for APLP1, APLP2, and BACE1. Anti-V5 antibody was used for TfR and anti-myc antibody for RHBDL4. β-actin was used as a loading control. Shown are representative blots of independent experiments (*i.e.* $n = 5$ for APLP1, APLP2, and TfR; $n = 3$ for BACE1). E, full-length APLP1 and APLP2 were normalized to β-actin and are shown as mean -fold change ± S.E. compared with inactive RHBDL4 set as 1. The quantification for APP was taken from Fig. 1*B* but is displayed as -fold-change. **, $p < 0.01$; ***, $p < 0.001$; two-tailed paired *t* test. *ecto*, ectodomain.

eral sites within the APP ectodomain, although we cannot exclude cleavage sites in transmembrane sequences or the involvement of another, still unknown protease. The active center of bacterial rhomboids has been localized to the extracellular face of the enzyme, forming an accessible cavity (30). Thus, artificial substrates such as casein can be cleaved by rhomboid proteases, although casein has no transmembrane sequence (29, 41). The ectodomain cleavage of APP by RHBDL4 described here is not unprecedented; however, the high number of APP cleavage sites is remarkable. It is currently unclear whether those cleavage events occur independently from each other or sequentially. If cleavage events occurred independently, we would anticipate finding 85- to 90-kDa APP ectodomain fragments corresponding to 10- to 15-kDa APP CTFs, which was not the case. The most abundant signals were the 70- to 73-kDa ectodomain fragments and the 22- to 25-kDa larger APP CTFs. Therefore, we reason that these fragments derive from processing at preferred cleavage sites (Figs. 1*H* and 5*D*). The soluble 70- to 73-kDa APP ectodomain fragments may be released from RHBDL4, whereas the transmembranous APP CTFs may remain bound to the enzyme and further trimmed, generating the smaller 10- to 15-kDa APP CTFs. At least for APP, it appears that RHBDL4 shows sheddase activity, implying that RHBDL4 exhibits dual "Janus"-like functionalities and mediates shedding of ectodomains as well as intramembrane cleavage in transmembrane sequences.

Recently, Fleck *et al.* (42) reported processing of neuregulin 1 by two different classes of intramembrane proteases, *i.e.* γ-secretase and signal peptide peptidase-like proteases. Our findings further support the idea that one substrate can be processed by two different classes of intramembrane proteases, *i.e.* in the case of APP, γ-secretase and RHBDL4, but we have not finally identified intramembrane cleavages by RHBDL4. Interestingly, RHBDL4 was also recently reported to cleave proTGFα even in the presence of the classical known sheddase TNFα-converting enzyme 1 (TACE) (23). In this context, RHBDL4 was up-regulated under the pathological condition of colorectal cancer, thus modulating EGF receptor signaling.

What might be the biological function of RHBDL4-mediated APP cleavage? One possibility could be that RHBDL4 controls the amount of full-length APP (and APLP1 and APLP2) at the cell surface via ER degradation (Fig. 5*D*). A similar mechanism was proposed in *Drosophila melanogaster* for the immature, membrane-bound EGF family ligands: they interact with iRhom (inactive rhomboid family members) in the ER, directing EGF toward proteasomal degradation and thus maintain low cell surface EGF levels (43). This notion is supported by our observation that the inactive mutant of RHBDL4 retained immature APP in the ER. Likewise, a recent publication by Wunderle *et al.* (44) suggests that RHBDL4 modulates the trafficking of several cell surface proteins.

As a consequence of RHBDL4-mediated APP cleavage in the ER, we showed that this pathway bypasses classical amyloidogenic APP processing and therefore drastically decreases Aβ levels (Fig. 5*D*), a finding that merits further investigation. However, the relevance of RHBDL4-mediated APP processing in Alzheimer disease pathology is currently unclear. Despite the decrease in Aβ, the accumulation of CTFs could be problematic as well (45). In addition, a recent paper described the formation of novel, toxic Aη fragments derived from larger APP CTFs (46). Future research will reveal whether RHBDL4 activity has protective or detrimental effects in Alzheimer disease pathology.

Conclusion—We show here that the APP family members are efficient substrates for the human rhomboid protease RHBDL4, implying that signal transduction conducted by the APP family is regulated by RHBDL4. RHBDL4-mediated APP processing furthers our understanding of the physiology of the APP family. Likewise, the highly efficient processing of APP, APLP1, and APLP2 by RHBDL4 may be useful in elucidating the cleavage mechanisms and kinetics of mammalian rhomboids.

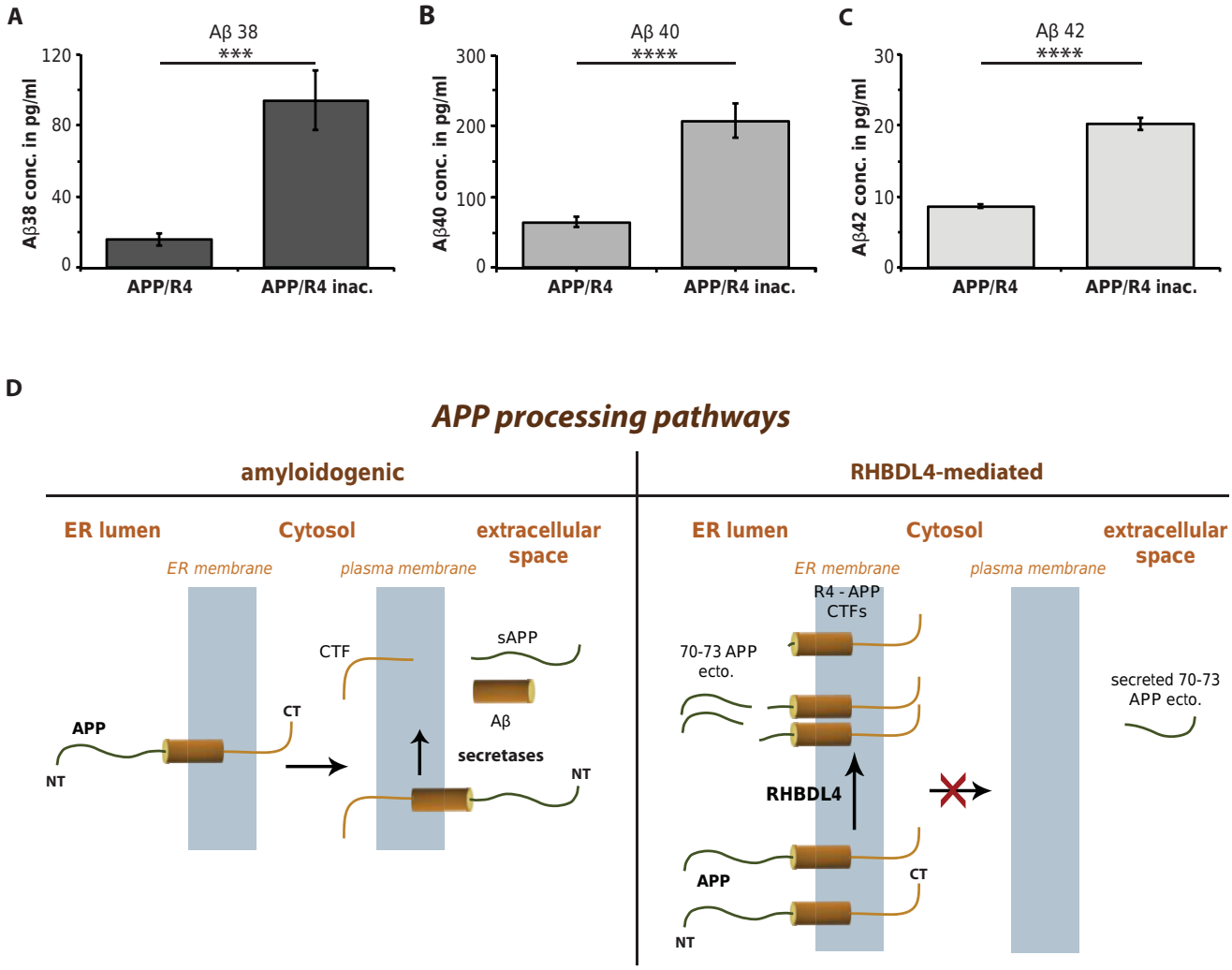

FIGURE 5. **RHBDL4 activity decreases Aβ38, Aβ40, and Aβ42 levels.** *A–C*, 36 h after transient transfection, fresh medium was conditioned for 24 h. Multiplex ELISA for Aβ38 (*A*), Aβ40 (*B*), and Aβ42 (*C*) was performed. Shown is the mean concentration (*conc*) in picograms per milliliter ± S.E. ($n = 4$). ***, $p < 0.001$; ****, $p < 0.0001$ (Bonferroni-corrected Student's *t* test). *D*, scheme of RHBDL4-mediated effects on APP processing. In the amyloidogenic APP processing model (*left panel*), APP is processed at the cell surface or in endosomes, where BACE1 and γ-secretase cleave APP to generate Aβ peptides. When RHBDL4 is processing APP (*right panel*), APP and RHBDL4 interact in the ER, where APP is cleaved multiple times by RHBDL4. Although the 70- to 73-kDa APP ectodomain (*ecto*) fragment likely accumulates inside the ER lumen and is partially secreted, the 22- to 25-kDa CTFs may be further trimmed by RHBDL4 generating 10- to 15-kDa APP CTFs. Consequently, less APP is transported to the cell surface and endosomes, preventing amyloidogenic APP processing and Aβ secretion.

Experimental Procedures

DNA Constructs—Plasmid pCMV6 containing the cDNAs encoding human RHBDL1–4 with a C-terminal myc-FLAG tag were obtained from OriGene. cDNAs encoding APP695 and APLP1 were cloned in pcDNA3.1 (Invitrogen) and APLP2 and BACE1 cDNA in pLBCX (Clontech). For co-immunoprecipitation analysis, an N-terminal myc tag was inserted after the signal peptide of APP695 in pcDNA3.1. cDNA encoding for the human transferrin receptor 1 was expressed from the pIRES vector with a C-terminal V5 tag. As mock controls, the empty vectors pcDNA3.1 or pCMV6 were used. Inactive RHBDL4 S144A was generated by site-directed mutagenesis using the forward primer 5′-gctgtaggtttcgcaggagttttgttt-3′ and reverse primer 5′-aaacaaaactcctgcgaaacctacagc-3′. All expression vectors were verified by dideoxy DNA sequencing (McGill Génome Québec Sequencing Center).

Cell Culture and Transfection—Most experiments were performed using HEK 293T cells cultivated in DMEM containing 4.5 g/liter glucose, 0.584 g/liter L-glutamine, and 0.11 g/liter sodium pyruvate (Wisent) and supplemented with 10% FCS (Wisent) at 37 °C and 5% CO_2. Cells were passaged at a confluency of 80–90%. For transient transfections, 6×10^5 cells/well (6-well plates) and 2×10^5 cells/well (12-well plates) were seeded 24 h before transfection, except for the ELISA (see below). Cells were transiently transfected with 2 μg of DNA in total and 4 μl of PEI (2 μg/μl) per 6 wells or 1 μg of DNA and 2 μl of PEI per 12 wells. For co-transfection, a DNA ratio of APP to rhomboid protease of 5:1 was used. 36 h after transfection, cells were lysed with TNE lysis buffer (50 mM Tris (pH 7.4), 150 mM NaCl, 2 mM EDTA, 1% Nonidet P-40, and complete protease inhibitors (Roche)) and prepared for SDS-PAGE. When SH-SY5Y cells were used, 8×10^5 cells were plated per 6 wells and transfected with 3 μg of DNA and 10 μl of Lipofectamine 2000 (Invitrogen). Cells were lysed 72 h after transfection with 100 μl of TNE lysis buffer and prepared for SDS-PAGE. For the detection of endogenous APP fragments, we followed the sam-

ple preparation according to Wang *et al.* (34) using approximately twice the protein load per lane compared with samples overexpressing APP.

Inhibitor Treatments—36 h after transfection, the cell culture medium was changed and supplemented with different inhibitors for 12 h. Inhibitor IV (Calbiochem) was used at 1 μM, L685,485 (Tocris) at a concentration of 1 μM, BB94 (Abcam) at 10 μM, ALLN (EMD Millipore) at 50 μM, phenanthroline at 100 μM (Sigma-Aldrich), and pepstatin A at 50 μM (Sigma-Aldrich). Treatment with E64D was performed for 24 h at 10 μM (Tocris). DMSO was used as a vehicle control. Cell supernatants were collected, and cells were lysed and prepared for SDS-PAGE analysis as outlined above.

Knockdown with shRNA—1×10^6 HEK 293T cells/10-cm dish were seeded and transfected with 8 μg of DNA and 16 μl of PEI. Psi-H1 plasmids encoding a shRNA against human RHBDL4 (ggacggcaatactactttaat) or a random non-targeting sequence as control under the H1 promoter as well as GFP under the human CMV promoter were transfected (GeneCopoeia). The GFP fluorescence was used to select for the top 40% of cells with brightest GFP signal with FACS. 36 h after transfection, cells were either treated for 12 h with 50 μM ALLN and then harvested with 3 ml of trypsin or first sorted by FACS, seeded again, and then treated with ALLN. Cells were resuspended in TNE lysis buffer at a concentration of 30,000 cells/μl, and lysates were analyzed on 4–12% bis-tris gels (Invitrogen).

Co-Immunoprecipitation—36 h after transfection, cells were lysed, and samples were diluted 1:1 with PBS. Immunoprecipitation was performed with 1.5 μg of 6E10 antibody at 4 °C overnight. After incubation with 30 μl of protein G-Sepharose for 4 h at 4 °C, samples were washed twice with washing buffer (50 mM Tris (pH 7.4), 150 mM NaCl, and 0.5% Nonidet P-40) and once with PBS. Sample buffer was added to the beads before SDS-PAGE analysis.

Western Blotting Analysis—Samples were separated on 10% or 15% Tris/glycine, 10–20% Tris/Tricine (Bio-Rad), or 4–12% bis-tris (NUPAGE, Invitrogen) SDS-PAGE gels (the latter two for APP CTFs) and transferred to nitrocellulose. The following primary antibodies were used: 22C11 (Millipore), LN27 (Invitrogen, APP epitope residues 45–53), 6E10 (Covance), C1/6.1 (BioLegend), anti-APP ab3 (Sigma-Aldrich, rabbit polyclonal, immunogen: 465–514 of APP695), mouse-anti-myc and rabbit-anti-myc (9B11 and 71D10, Cell Signaling Technology), mouse-anti-β-actin (8H10D10, Cell Signaling Technology), rabbit-anti-GAPDH (^{14}C10, Cell Signaling Technology), rabbit-anti-sAPPβ (IBL), rabbit-anti-V5 (D3H8Q, Cell Signaling Technology), mouse-anti-BACE1 (D10E5, Cell Signaling Technology), rabbit-anti-APLP1 (ab192481, Abcam), rabbit anti-APLP2 (ab128603, Abcam), rabbit-anti-RHBDL4 (HPA013972, Sigma-Aldrich), rabbit-anti-LC3B (2775, Cell Signaling Technology). HRP-coupled secondary antibodies directed against mouse or rabbit IgG were purchased from Promega. Chemiluminescence images were acquired using the digital ImageQuant LAS 500 system (GE Healthcare).

ELISA—4.5×10^5 HEK 293T cells were seeded per well in 6-well plates 24 h prior to transfection. Cells were transfected with 2 μg of DNA and 4 μl of PEI per well. 36 h after transfection, the medium was replaced and conditioned for 24 h. Cell debris was pelleted from supernatant by centrifugation at $10{,}000 \times g$ for 10 min. Aβ38, Aβ40, and Aβ42 levels were quantified using the Meso Scale Discovery immunogenicity assay according to the instructions of the manufacturer. Corresponding cells were lysed to control for equal transfection levels by Western blotting.

Data analysis and Statistics—Western blotting images were quantified with ImageJ. Statistical data analysis was performed with GraphPad Prism 6.

Author Contributions—S. P. designed and performed the majority of experiments, analyzed data, and wrote the first draft of the manuscript. M. H., F. O. designed and performed experiments and contributed to the manuscript. L. M. M. led the research, designed experiments, and wrote the manuscript.

Acknowledgments—We thank Dr. Matthew Freeman and Dr. Jason Young for critically reviewing the manuscript and Dr. Claus Pietrzik and Dr. Nabil Seidah for plasmid cDNAs. We thank Meijuan Niu for help with DNA cloning.

References

1. Puig, K. L., and Combs, C. K. (2013) Expression and function of APP and its metabolites outside the central nervous system. *Exp. Gerontol.* **48,** 608–611
2. Multhaup, G., Schlicksupp, A., Hesse, L., Beher, D., Ruppert, T., Masters, C. L., and Beyreuther, K. (1996) The amyloid precursor protein of Alzheimer's disease in the reduction of copper(II) to copper(I). *Science* **271,** 1406–1409
3. Pierrot, N., Tyteca, D., D'auria, L., Dewachter, I., Gailly, P., Hendrickx, A., Tasiaux, B., Haylani, L. E., Muls, N., N'kuli, F., Laquerrière, A., Demoulin, J. B., Campion, D., Brion, J. P., Courtoy, P. J., *et al.* (2013) Amyloid precursor protein controls cholesterol turnover needed for neuronal activity. *EMBO Mol. Med.* **5,** 608–625
4. van der Kant, R., and Goldstein, L. S. (2015) Cellular functions of the amyloid precursor protein from development to dementia. *Dev. Cell* **32,** 502–515
5. Kamenetz, F., Tomita, T., Hsieh, H., Seabrook, G., Borchelt, D., Iwatsubo, T., Sisodia, S., and Malinow, R. (2003) APP processing and synaptic function. *Neuron* **37,** 925–937
6. Priller, C., Bauer, T., Mitteregger, G., Krebs, B., Kretzschmar, H. A., and Herms, J. (2006) Synapse formation and function is modulated by the amyloid precursor protein. *J. Neurosci.* **26,** 7212–7221
7. Young-Pearse, T. L., Bai, J., Chang, R., Zheng, J. B., LoTurco, J. J., and Selkoe, D. J. (2007) A critical function for β-amyloid precursor protein in neuronal migration revealed by *in utero* RNA interference. *J. Neurosci.* **27,** 14459–14469
8. Heber, S., Herms, J., Gajic, V., Hainfellner, J., Aguzzi, A., Rülicke, T., von Kretzschmar, H., von Koch, C., Sisodia, S., Tremml, P., Lipp, H. P., Wolfer, D. P., and Müller, U. (2000) Mice with combined gene knock-outs reveal essential and partially redundant functions of amyloid precursor protein family members. *J. Neurosci.* **20,** 7951–7963
9. Eggert, S., Paliga, K., Soba, P., Evin, G., Masters, C. L., Weidemann, A., and Beyreuther, K. (2004) The proteolytic processing of the amyloid precursor protein gene family members APLP-1 and APLP-2 involves α-, β-, γ-, and ϵ-like cleavages: modulation of APLP-1 processing by *N*-glycosylation. *J. Biol. Chem.* **279,** 18146–18156
10. Li, Q., and Südhof, T. C. (2004) Cleavage of amyloid-β precursor protein and amyloid-β precursor-like protein by BACE 1. *J. Biol. Chem.* **279,** 10542–10550
11. De Strooper, B., Saftig, P., Craessaerts, K., Vanderstichele, H., Guhde, G., Annaert, W., Von Figura, K., and Van Leuven, F. (1998) Deficiency of presenilin-1 inhibits the normal cleavage of amyloid precursor protein. *Nature* **391,** 387–390

12. Viola, K. L., and Klein, W. L. (2015) Amyloid β oligomers in Alzheimer's disease pathogenesis, treatment, and diagnosis. *Acta Neuropathol.* **129,** 183–206
13. Lichtenthaler, S. F., Haass, C., and Steiner, H. (2011) Regulated intramembrane proteolysis: lessons from amyloid precursor protein processing. *J. Neurochem.* **117,** 779–796
14. Freeman, M. (2014) The rhomboid-like superfamily: molecular mechanisms and biological roles. *Annu. Rev. Cell Dev. Biol.* **30,** 235–254
15. Kinch, L. N., and Grishin, N. V. (2013) Bioinformatics perspective on rhomboid intramembrane protease evolution and function. *Biochim. Biophys. Acta* **1828,** 2937–2943
16. Lemberg, M. K., and Freeman, M. (2007) Functional and evolutionary implications of enhanced genomic analysis of rhomboid intramembrane proteases. *Genome Res.* **17,** 1634–1646
17. Adrain, C., Strisovsky, K., Zettl, M., Hu, L., Lemberg, M. K., and Freeman, M. (2011) Mammalian EGF receptor activation by the rhomboid protease RHBDL2. *EMBO Rep.* **12,** 421–427
18. Adrain, C., Zettl, M., Christova, Y., Taylor, N., and Freeman, M. (2012) Tumor necrosis factor signaling requires iRhom2 to promote trafficking and activation of TACE. *Science* **335,** 225–228
19. Christova, Y., Adrain, C., Bambrough, P., Ibrahim, A., and Freeman, M. (2013) Mammalian iRhoms have distinct physiological functions including an essential role in TACE regulation. *EMBO Rep.* **14,** 884–890
20. Hosur, V., Johnson, K. R., Burzenski, L. M., Stearns, T. M., Maser, R. S., and Shultz, L. D. (2014) Rhbdf2 mutations increase its protein stability and drive EGFR hyperactivation through enhanced secretion of amphiregulin. *Proc. Natl. Acad. Sci. U.S.A.* **111,** E2200-E2209
21. Liao, H. J., and Carpenter, G. (2012) Regulated intramembrane cleavage of the EGF receptor. *Traffic* **13,** 1106–1112
22. Siggs, O. M., Xiao, N., Wang, Y., Shi, H., Tomisato, W., Li, X., Xia, Y., and Beutler, B. (2012) iRhom2 is required for the secretion of mouse TNFα. *Blood* **119,** 5769–5771
23. Song, W., Liu, W., Zhao, H., Li, S., Guan, X., Ying, J., Zhang, Y., Miao, F., Zhang, M., Ren, X., Li, X., Wu, F., Zhao, Y., Tian, Y., Wu, W., *et al.* (2015) Rhomboid domain containing 1 promotes colorectal cancer growth through activation of the EGFR signalling pathway. *Nat. Commun.* **6,** 8022
24. Jin, S. M., Lazarou, M., Wang, C., Kane, L. A., Narendra, D. P., and Youle, R. J. (2010) Mitochondrial membrane potential regulates PINK1 import and proteolytic destabilization by PARL. *J. Cell Biol.* **191,** 933–942
25. Meissner, C., Lorenz, H., Weihofen, A., Selkoe, D. J., and Lemberg, M. K. (2011) The mitochondrial intramembrane protease PARL cleaves human Pink1 to regulate Pink1 trafficking. *J. Neurochem.* **117,** 856–867
26. Shi, G., Lee, J. R., Grimes, D. A., Racacho, L., Ye, D., Yang, H., Ross, O. A., Farrer, M., McQuibban, G. A., and Bulman, D. E. (2011) Functional alteration of PARL contributes to mitochondrial dysregulation in Parkinson's disease. *Hum. Mol. Genet.* **20,** 1966–1974
27. Urban, S., Lee, J. R., and Freeman, M. (2001) *Drosophila* rhomboid-1 defines a family of putative intramembrane serine proteases. *Cell* **107,** 173–182
28. Maegawa, S., Koide, K., Ito, K., and Akiyama, Y. (2007) The intramembrane active site of GlpG, an *E. coli* rhomboid protease, is accessible to water and hydrolyses an extramembrane peptide bond of substrates. *Mol. Microbiol.* **64,** 435–447
29. Strisovsky, K., Sharpe, H. J., and Freeman, M. (2009) Sequence-specific intramembrane proteolysis: identification of a recognition motif in rhomboid substrates. *Mol. Cell* **36,** 1048–1059
30. Wang, Y., Zhang, Y., and Ha, Y. (2006) Crystal structure of a rhomboid family intramembrane protease. *Nature* **444,** 179–180
31. Xue, Y., and Ha, Y. (2012) Catalytic mechanism of rhomboid protease GlpG probed by 3,4-dichloroisocoumarin and diisopropyl fluorophosphonate. *J. Biol. Chem.* **287,** 3099–3107
32. Bergbold, N., and Lemberg, M. K. (2013) Emerging role of rhomboid family proteins in mammalian biology and disease. *Biochim. Biophys. Acta* **1828,** 2840–2848
33. Fleig, L., Bergbold, N., Sahasrabudhe, P., Geiger, B., Kaltak, L., and Lemberg, M. K. (2012) Ubiquitin-dependent intramembrane rhomboid protease promotes ERAD of membrane proteins. *Mol. Cell* **47,** 558–569
34. Wang, H., Sang, N., Zhang, C., Raghupathi, R., Tanzi, R. E., and Saunders, A. (2015) Cathepsin L mediates the degradation of novel APP C-terminal fragments. *Biochemistry* **54,** 2806–2816
35. Kuhn, P. H., Wang, H., Dislich, B., Colombo, A., Zeitschel, U., Ellwart, J. W., Kremmer, E., Rossner, S., and Lichtenthaler, S. F. (2010) ADAM10 is the physiologically relevant, constitutive α-secretase of the amyloid precursor protein in primary neurons. *EMBO J.* **29,** 3020–3032
36. Blaydon, D. C., Etheridge, S. L., Risk, J. M., Hennies, H. C., Gay, L. J., Carroll, R., Plagnol, V., McRonald, F. E., Stevens, H. P., Spurr, N. K., Bishop, D. T., Ellis, A., Jankowski, J., Field, J. K., Leigh, I. M., *et al.* (2012) RHBDF2 mutations are associated with tylosis, a familial esophageal cancer syndrome. *Am. J. Hum. Genet.* **90,** 340–346
37. Issuree, P. D., Maretzky, T., McIlwain, D. R., Monette, S., Qing, X., Lang, P. A., Swendeman, S. L., Park-Min, K. H., Binder, N., Kalliolias, G. D., Yarilina, A., Horiuchi, K., Ivashkiv, L. B., Mak, T. W., Salmon, J. E., and Blobel, C. P. (2013) iRHOM2 is a critical pathogenic mediator of inflammatory arthritis. *J. Clin. Invest.* **123,** 928–932
38. Halliday, M., and Mallucci, G. R. (2014) Targeting the unfolded protein response in neurodegeneration: a new approach to therapy. *Neuropharmacology* **76,** 169–174
39. Plácido, A. I., Pereira, C. M., Duarte, A. I., Candeias, E., Correia, S. C., Santos, R. X., Carvalho, C., Cardoso, S., Oliveira, C. R., and Moreira, P. I. (2014) The role of endoplasmic reticulum in amyloid precursor protein processing and trafficking: implications for Alzheimer's disease. *Biochim. Biophys. Acta* **1842,** 1444–1453
40. Vella, L. J., and Cappai, R. (2012) Identification of a novel amyloid precursor protein processing pathway that generates secreted N-terminal fragments. *FASEB J.* **26,** 2930–2940
41. Lazareno-Saez, C., Arutyunova, E., Coquelle, N., and Lemieux, M. J. (2013) Domain swapping in the cytoplasmic domain of the *Escherichia coli* rhomboid protease. *J. Mol. Biol.* **425,** 1127–1142
42. Fleck, D., Voss, M., Brankatschk, B., Giudici, C., Hampel, H., Schwenk, B., Edbauer, D., Fukumori, A., Steiner, H., Kremmer, E., Haug-Kröper, M., Rossner, M. J., Fluhrer, R., Willem, M., and Haass, C. (2016) Proteolytic processing of neuregulin 1 type III by three intramembrane-cleaving proteases. *J. Biol. Chem.* **291,** 318–333
43. Zettl, M., Adrain, C., Strisovsky, K., Lastun, V., and Freeman, M. (2011) Rhomboid family pseudoproteases use the ER quality control machinery to regulate intercellular signaling. *Cell* **145,** 79–91
44. Wunderle, L., Knopf, J. D., Kühnle, N., Morlé, A., Hehn, B., Adrain, C., Strisovsky, K., Freeman, M., and Lemberg, M. K. (2016) Rhomboid intramembrane protease RHBDL4 triggers ER-export and non-canonical secretion of membrane-anchored TGFα. *Sci. Rep.* **6,** 27342
45. Mitani, Y., Yarimizu, J., Saita, K., Uchino, H., Akashiba, H., Shitaka, Y., Ni, K., and Matsuoka, N. (2012) Differential effects between γ-secretase inhibitors and modulators on cognitive function in amyloid precursor protein-transgenic and nontransgenic mice. *J. Neurosci.* **32,** 2037–2050
46. Willem, M., Tahirovic, S., Busche, M. A., Ovsepian, S. V., Chafai, M., Kootar, S., Hornburg, D., Evans, L. D., Moore, S., Daria, A., Hampel, H., Müller, V., Giudici, C., Nuscher, B., Wenninger-Weinzierl, A., *et al.* (2015) η-Secretase processing of APP inhibits neuronal activity in the hippocampus. *Nature* **526,** 443–447